

## DELINEATION OF THE UNDERGROUND STRUCTURE USING 2D GRAVITY DATA MODELLING IN GEOTHERMAL POTENTIAL AREA AS AN ANALYSIS OF SUSTAINABLE ENERGY EXPLORATION STRATEGIES

TRISNA IKHSAN NINGATI<sup>1,\*</sup>, MUHAMAD RAGIL SETIAWAN<sup>1</sup>  
RAHMAT NAWI SIREGAR<sup>1</sup>, ALAMTA SINGARIMBUN<sup>2</sup>, EMI PRASETYAWATI UMAR<sup>3</sup>  
ROFIQUL UMAM<sup>4</sup> AND HIROTAKA TAKAHASHI<sup>5</sup>

<sup>1</sup>Department of Physics  
Institut Teknologi Sumatera  
Jalan Terusan Ryacudu, Jati Agung, South Lampung Regency, Lampung 35365, Indonesia  
{ragil.setiawan; rahmat.siregar}@fi.itera.ac.id  
\*Corresponding author: trisna.224100001@student.itera.ac.id

<sup>2</sup>Department of Physics  
Faculty of Mathematics and Natural Sciences  
Institut Teknologi Bandung  
Jalan Ganesa 10 Bandung, East Java 40132, Indonesia  
alamta@fi.itb.ac.id

<sup>3</sup>Department of Mining Engineering  
Universitas Muslim Indonesia  
Jalan Urip Sumoharjo 14 Makassar, South Sulawesi 90231, Indonesia  
emiprasyawati.umar@umi.ac.id

<sup>4</sup>Faculty of Life and Environmental Sciences  
University of Tsukuba  
1-1-1, Tennodai, Tsukuba, Ibaraki 305-8577, Japan  
rofiqul.umam.ft@u.tsukuba.ac.jp

<sup>5</sup>Research Center for Space Science, Advanced Research Laboratories  
Department of Design and Data Science  
Tokyo City University  
3-3-1, Ushikubo-Nishi, Tsuzuki-Ku, Yokohama, Kanagawa 224-8551, Japan  
hirotaka@tcu.ac.jp

Received June 2025; accepted August 2025

**ABSTRACT.** *The increasing demand for sustainable energy has intensified the search for viable geothermal resources, necessitating advanced geophysical methods for efficient exploration. In the Sekincau Timur, Becingut, located between Batubrak District and Bandar Negeri Suoh District, West Lampung Regency, Lampung Province, Indonesia, has geothermal potential. This potential can be utilized and developed as a renewable and sustainable energy source. However, before exploitation and exploration can take place, an initial analysis of the subsurface structure is required to determine the location of geothermal potential in the area, in other words, delineation. This study aims to determine the patterns of gravity anomalies, rock density contrasts, and subsurface structures of the Sekincau Timur geothermal field in Lampung Province, Indonesia. In this study, the subsurface structure will be modelled in 2D with secondary data from residual anomalies and regional topography experiment (TOPEX) anomalies. The results of the study indicate that the gravity anomaly patterns exhibit low variation with a rock density range*

of 1.00-2.55 g/cm<sup>3</sup>, moderate variation with a rock density range of 2.22-2.76 g/cm<sup>3</sup>, and high variation with a rock density range of 2.72-3.00 g/cm<sup>3</sup>. 2D modelling produced a subsurface structure in the form of a fault with a direction from the northwest to the southeast and from the northeast to the southwest, with topsoil at a depth of 0.00-0.11 km, caprock (cover rock) at a depth of 0.20 km, the reservoir is at a depth of 1.20-1.60 km, the recharge area (where meteoric water enters) is at a depth of 0.30 km, and a pull-apart basin is at a depth of 0.40 km. The results highlight the correlation between gravity anomalies and geothermal activity, offering insights into optimal drilling targets and long-term energy extraction feasibility. This analysis not only contributes to geophysical exploration methodologies but also reinforces the importance of integrating gravity data with multidisciplinary approaches for responsible geothermal development.

**Keywords:** 2D gravity data modeling, Residual and regional anomaly, Rock density, Potential geothermal, Eastern Sekincau

**1. Introduction.** Geothermal energy is one of the most abundant renewable energy sources in Indonesia, owing to its unique geological position at the convergence of the Eurasian, Australian, and Pacific tectonic plates. This tectonic interaction places Indonesia within the Ring of Fire, a chain of active volcanoes that serves as a rich source of geothermal energy [1]. According to surveys by the Geological Agency of the Ministry of Energy and Mineral Resources, there are 331 geothermal potential sites distributed across Sumatra, Java, Bali, Nusa Tenggara, and Maluku [2]. Sumatra holds the highest potential, estimated at 12 GW, with 93 identified sites, including several in Lampung Province [3].

As a promising renewable resource, geothermal energy plays a vital role in the global transition toward sustainable energy. Indonesia, being one of the most geothermal-rich regions in the world, offers vast opportunities for exploration and development [4,5]. The Eastern Sekincau area in Lampung Province exemplifies this potential, characterized by complex geological structures and favorable subsurface conditions [6-8]. Understanding subsurface structures is essential in geothermal exploration, as it helps identify reservoirs, heat sources, and fluid pathways. One effective geophysical method for this purpose is gravity surveying, which detects variations in the gravitational field caused by differences in rock density [9,10]. This method is particularly useful for mapping bedrock, intrusions, fault zones, and other geological formations [11].

Gravity data modeling has become a powerful tool for visualizing subsurface features, offering insights into density contrasts and fault structures that influence geothermal systems [9,10,12]. In this study, a two-dimensional (2D) gravity model is employed to interpret gravity anomalies and rock density distributions in the Eastern Sekincau region. These anomalies help delineate subsurface structures, such as fault orientations, caprock layers, and reservoir depths [9,13-16]. This research aims to delineate the geothermal structure of Eastern Sekincau using 2D gravity modeling. The results will enhance understanding of the area's geological framework and support efficient resource exploitation [9,10,12,17]. By integrating advanced geophysical techniques, the study contributes to Indonesia's renewable energy goals and advances global methodologies in geothermal exploration.

## 2. Methodologies.

**2.1. Location.** The Sekincau Timur area is located and composed of several formations, namely the Ranau Formation originating from Suoh (QTrs), the Old Quaternary Volcanic Rock Formation (Qv), the Young Quaternary Volcanic Rock Formation originating from Sekincau (Qhvs) and Bukit Penetoh (Qhvh), and the Alluvium Formation (Qa), which is the youngest deposit originating from the Way Semangka River [3]. There are also scattered alignments from the northwest to the southeast, as mapped on the

regional geological map. The research was conducted and focused on the coordinates 5°6'11.91'-5°13'37.19'LS and 104°11'17.35"-104°25'25.53'E with the study area being the Sekincau Timur geothermal field, Becingut, Batubrak District, Bandar Negeri Suoh District, West Lampung Regency, Lampung Province, Indonesia, using secondary data obtained from the TOPEX satellite (Figure 1).

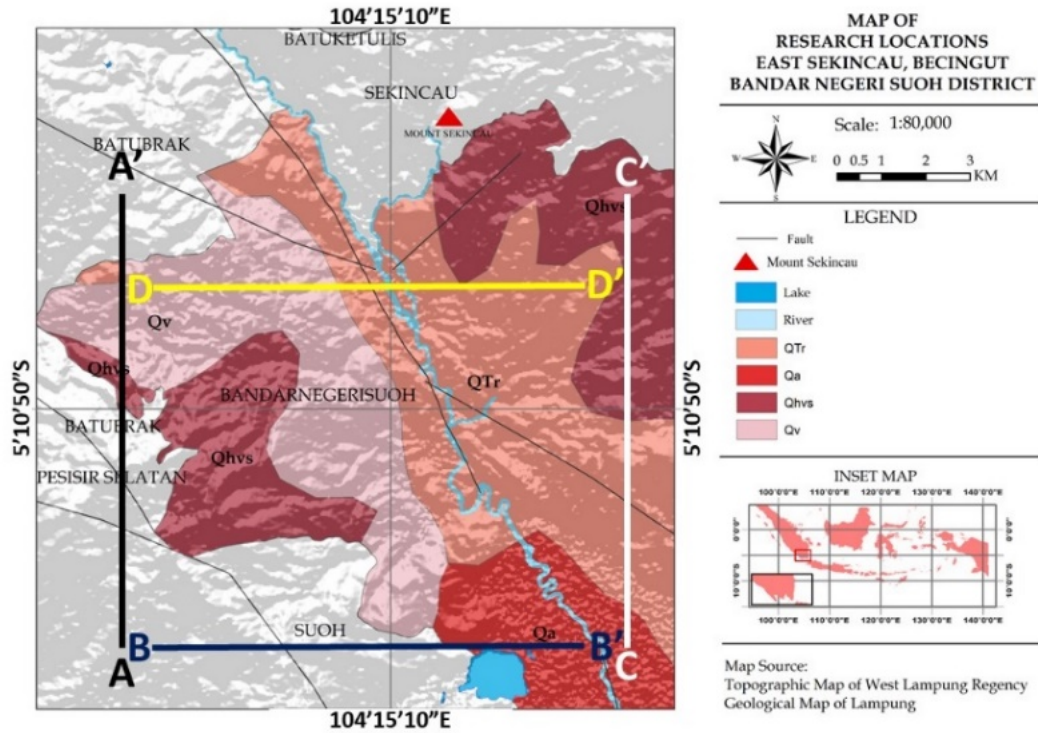


FIGURE 1. Regional geological map of East Sekincau, Becingut, Batubrak Subdistrict, Bandar Negeri Suoh Subdistrict, West Lampung Regency, Lampung Province, Indonesia

**2.2. Principles of the gravity and analytical method.** The gravitational method is based on Newton’s law of gravitation, which states that the gravitational force between two materials with different masses,  $m_0$  and  $m$ , separated by a distance  $|\vec{r} - \vec{r}_0|$  from the centre of mass is proportional to the product of the different masses and inversely proportional to the square of the distance (Figure 2), which can be written in Equation (1).

$$\vec{F}(\vec{r}) = -G \frac{m_0 m (\vec{r} - \vec{r}_0)}{|\vec{r} - \vec{r}_0|^2 |\vec{r} - \vec{r}_0|} \quad (1)$$

$\vec{F}(\vec{r})$  is the force acting on  $m$  due to the presence of  $m_0$  in the opposite direction, namely  $|\vec{r} - \vec{r}_0|$  where  $m_0$  in meters.  $G$  is the gravitational constant with a magnitude  $6.67428 \times 10^{11} \text{ Nm}^2\text{kg}^{-2}$ . Gravitational field is a measurable quantity in gravitational methods. The gravitational field of material  $m_0$  is the magnitude of the force per unit mass at a point at a distance  $|\vec{r} - \vec{r}_0|$  from  $m$ , which can be written in Equation (2).

$$\vec{E}(\vec{r}) = \frac{\vec{F}(\vec{r})}{m(\vec{r})} = G \frac{m_0 m (\vec{r} - \vec{r}_0)}{|\vec{r} - \vec{r}_0|^2 |\vec{r} - \vec{r}_0|} \quad (2)$$

$\vec{E}(\vec{r})$  is the gravitational field,  $m_0$  is the mass of the material, and  $|\vec{r} - \vec{r}_0|$  the distance between the point and the centre of mass. The gravitational potential of a collection of masses is the sum of the gravitational forces of each mass [12]. The sum of the vectors of the potentials caused by the masses in space is the total force on the material being

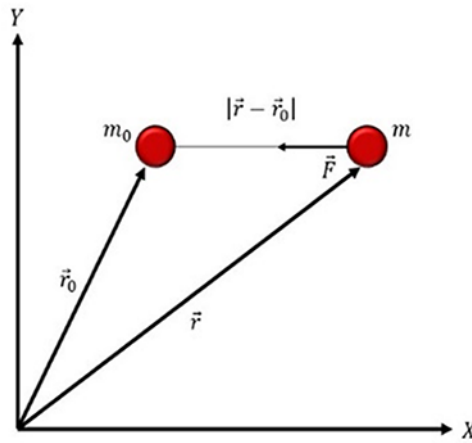


FIGURE 2. Attractive force between two materials

tested. The gravitational force at the boundary of a continuous mass distribution  $m$  can be determined using this principle [18]. A continuous mass distribution  $m$  is a collection of very small masses in very large numbers,  $dm = (x, y, z)$ , which is the density of the mass distribution. The application of the superposition principle can be written in Equation (3).

$$U(P) = \gamma \int_v \frac{dm}{r} = \gamma \int_v \frac{\rho(Q)}{r} dv \tag{3}$$

The integration covers the volume where the actual volume is located in the mass.  $U$  is the gravitational potential,  $\gamma$  is the gravitational constant,  $P$  is the observation point,  $Q$  is the integration point,  $r$  is the distance between  $P$  and  $Q$ ,  $\rho$  is density distribution, and the density is in units of  $\text{g/cm}^3$ . The observation point located outside the mass distribution (Figure 3) must be considered. If the density of the mass distribution is good, then the integration in Equation (3) is convergent for all  $P$  outside the mass, and the differentials  $x, y, z$  can be transformed into integral form.

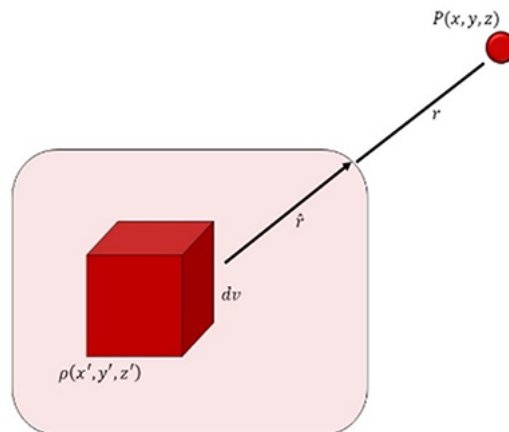


FIGURE 3. Gravitational force at point  $P$  due to density distribution  $\rho$

The Bouguer gravity anomaly (BGA) method employs several equations to calculate gravity anomalies by taking account of three stages of correction [11]. The first is Free-Air Correction (FAC). This stage is performed to eliminate the topographical or height effects that affect the reading value of the weight force value without considering the effect of the rock mass [19,20]. The second stage is the Bouguer Correction (BC), which is an elevation correction that takes account of the effect of the mass of rock between the

datum surface (geoid) and the survey point. The third stage is Topographic Correction (TC). This correction is made to consider the gravitational field effect of the surrounding topography. During measurement, the topographic elevation around the measurement point, usually within the inner and outer radius, is measured.

### 3. Main Results.

**3.1. Topographic overlay map with Bouguer gravity anomalies (BGA).** A topographic overlay map with BGA represents the spatial distribution of rock density variations beneath the surface [10]. Figure 4 illustrates the BGA values across the study area, ranging from 64 to 110 mGal. High anomalies (96-110 mGal, orange to red) correspond to high-density rocks in elevated regions, medium anomalies (76-94 mGal, light green to yellow) indicate medium-density rocks in flat terrains, and low anomalies (62-74 mGal, purple to blue) are associated with low-density rocks in lowland areas. Further geological insights can be obtained through processing techniques such as anomaly separation and 2D modeling.

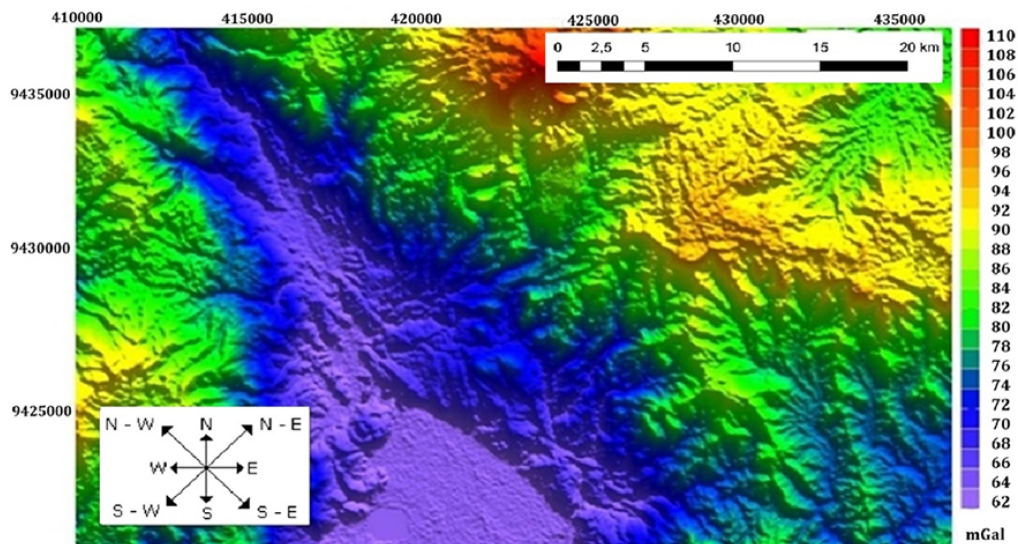


FIGURE 4. Topographic overlay map with Bouguer gravity anomaly values. Low anomalies (62-74 mGal): Indicates low-lying areas or zones with light sedimentary rocks, may indicate the presence of caprock or fluid zones. Medium anomalies (76-94 mGal): Generally found in flat areas, indicating medium-density igneous or metamorphic rocks, may indicate a transition between the reservoir zone and the caprock zone. High anomaly (96-110 mGal): Associated with high-density rocks such as magmatic intrusions or hard bedrock, often associated with geothermal heat sources or fault structures.

Bouguer gravity anomalies in the study area vary due to topographic differences, introducing distortions in the measurements [4]. To correct for these variations, the anomalies are reduced to a flat surface using the Dampney method implemented in matrix laboratory (MATLAB) 2010 [21]. Figure 5 presents the BGA map after this correction, employing an average topographic elevation of 1,451 m and an equivalent source depth of 8,500 m above sea level.

The results of the reduction showed a range of 62-106 mGal with a similar anomaly pattern but smoother contours and a smaller range than the Bouguer gravity anomaly in the topography. The difference is estimated to be due to the influence of the depth of the equivalent source of mass points and the average elevation used, and the gravity anomaly values are related to these two factors. During the reduction process to a flat

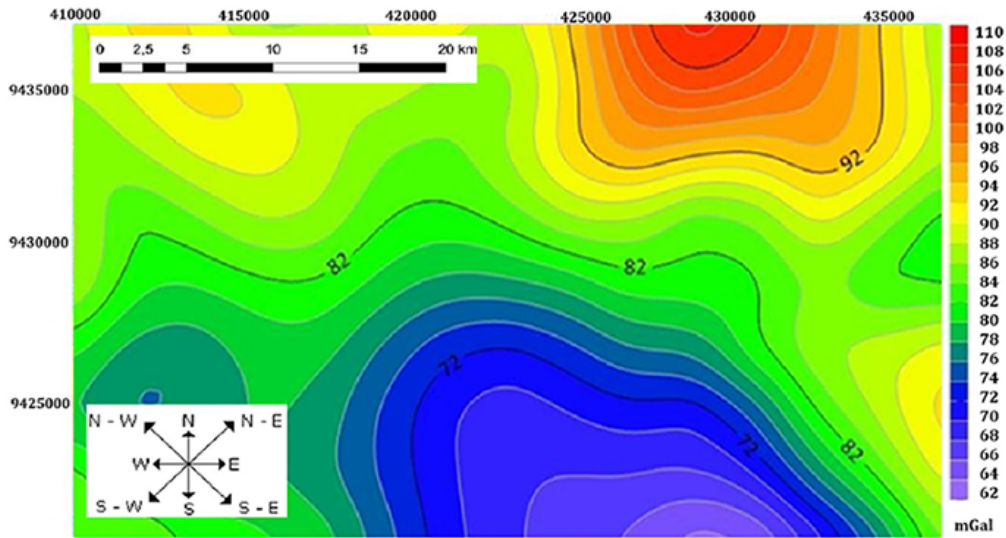


FIGURE 5. BGA map on a flat surface

surface using varying equivalent source heights and depths, such as 6,500, 7,000, 7,500, 8,000, 8,500, and 9,000 mdpl. At a depth of 8,500 mdpl, it is estimated to be close to the Bouguer gravity anomaly pattern on the topographic overlay map (Figure 4). The anomaly pattern shown on the BGA map in the flat surface (Figure 5) indicates high anomalies (orange-red colours) with a range of 96-110 mGal, moderate anomalies (light green-yellow colours) with a range of 76-94 mGal, and low anomalies (dark blue-light blue colours) with a range of 62-74 mGal. Within these anomalies, regional anomalies and residual anomalies can be separated to determine the anomaly depths to be used in the 2D modelling process.

**3.2. Spectrum analysis.** Spectrum analysis is the process of calculating and analyzing graphs generated after obtaining a complete Bouguer anomaly map in a flat field by utilizing part of the Fourier transform, namely the fast Fourier transform (FFT), which will produce a radially average power spectrum (RAPS) graph (Figure 6) so that the depth of regional anomalies, residual anomalies and noise can be determined [22].

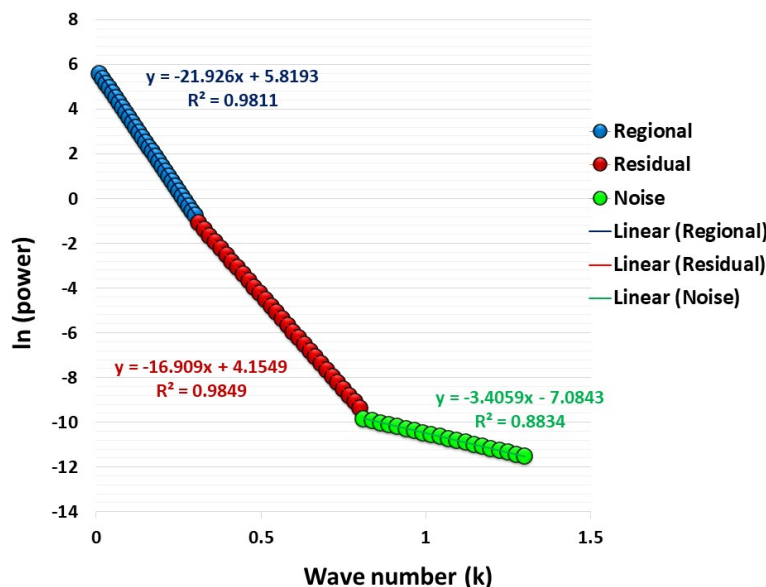


FIGURE 6. The radially average power spectrum (RAPS) graph

The depth of the anomaly will be used as the depth limit in the creation of 2D models. The slope found in each anomaly section is  $y = -21.926x + 5.8193$  with  $R^2 = 0.9811$  (regional anomaly),  $y = -16.909x + 4.1549$  with  $R^2 = 0.9849$  (residual anomaly),  $y = -3.4059x - 7.0843$  with  $R^2 = 0.8834$  (*noise*).  $R^2$  is the coefficient of determination, which indicates that the regional anomaly and residual values are close to 1. This indicates that the wave number ( $k$ ) and  $\text{Ln}(A)$  data are influenced by 98.11% and 1.89% by other variables (regional anomalies), and the wave number ( $k$ ) and  $\text{Ln}(A)$  data are influenced by 98.49% and 1.51% by other variables (residual anomalies).

Compared to these studies, the East Sekincau region exhibits a broader and higher anomaly range (64-110 mGal), suggesting the presence of denser rock formations and deeper geothermal reservoirs. Furthermore, the integration of the Dampney reduction method and FFT-based spectrum analysis in this study offers enhanced precision in determining anomaly depths an approach not fully adopted in the aforementioned studies. This highlights the value of combining topographic correction and spectral techniques to improve subsurface interpretation and support more efficient geothermal exploration [23].

**3.3. Separation of regional anomalies and residual anomalies.** Anomaly separation is performed to determine the source of the anomaly or the depth of the anomaly using one of the methods, namely the moving average method. During the separation process, two anomalies are produced: a deeper anomaly known as the regional anomaly (Figure 7) and a shallower anomaly known as the residual anomaly (Figure 8), obtained by subtracting the complete Bouguer anomaly from the regional anomaly. The moving average method is used in anomaly separation because the resulting anomaly patterns are clearer and more regular compared to other separation methods such as the Gaussian method and high pass filter. Figure 7 shows a regional anomaly map, which depicts deeper subsurface structures.

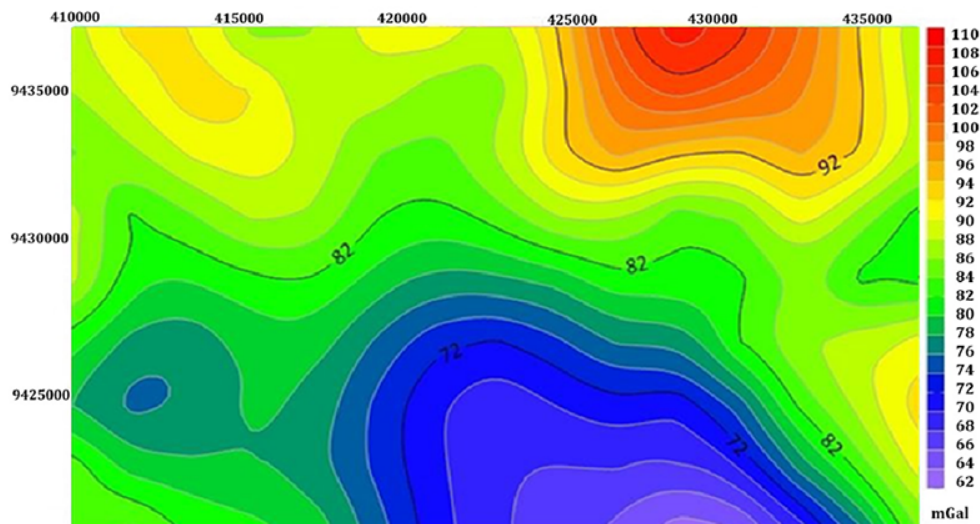


FIGURE 7. Regional anomaly map after the separation process (deeper)

The results of the anomaly separation show that the regional anomaly pattern has a range of 64 to 110 mGal. The anomaly values are the same, but the contours produced are not as smooth as the complete Bouguer anomaly on a flat surface. The anomaly patterns shown on the map are high, medium, and low anomalies. High anomalies have a range of 96-110 mGal, medium anomalies have a range of 76-94 mGal, and low anomalies have a range of 62-74 mGal. Figure 8 shows the residual anomaly map, which depicts shallow subsurface structures. The results of anomaly separation indicate that the residual anomaly pattern has a range of  $-1$  to  $1.1$  mGal. Negative residual anomaly values indicate

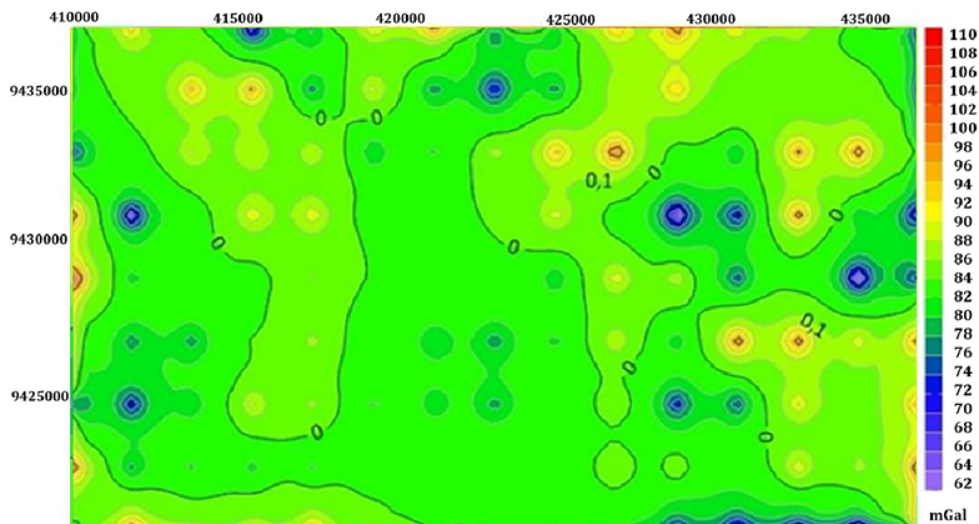


FIGURE 8. Residual anomaly map after the separation process (shallower)

that the rocks in the study area have shallower depths with varying density differences. The anomaly patterns shown on the map are high, medium and low anomalies. High anomalies (orange-red) with a range of 0.6 to 1.1 mGal, medium anomalies (light green-yellow) with a range of  $-0.1$  to 0.3 mGal and low anomalies (purple-blue) with a range of  $-1$  to  $-0.2$  mGal.

**3.4. Interpretation of 2D models.** The resulting 2D model consists of intersections along the X- and Y-axes, with cross-sections selected to best represent the subsurface conditions of the study area, which is primarily controlled by fault structures. Figure 1 shows the positions of these cross-sections correlated with the regional geological map. Cross-section A-A' at X = 417.52, illustrated in Figure 9, crosses the Batubrak sub-district, including Qhvs, Qv, and QTr formations. This section contains two northwest-southeast-oriented strike-slip faults, located between latitudes 9422-9429 and 9429-9436, extending from area A to B at a depth of 0.30 km. These faults, evident through minor block subsidence and permeable rock formations (dark blue-light green anomalies), are part of the Semangko segment of the Sumatra fault, influencing geothermal potential in the region. The uppermost layer comprises low-density topsoil ( $1.89 \text{ g/cm}^3$ ) in area A from

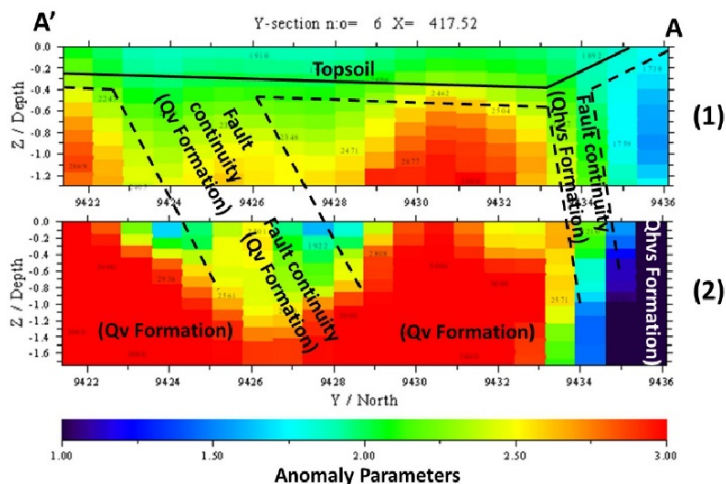


FIGURE 9. Cross-section of section A'-A data residual anomalies (1) and regional anomalies (2)

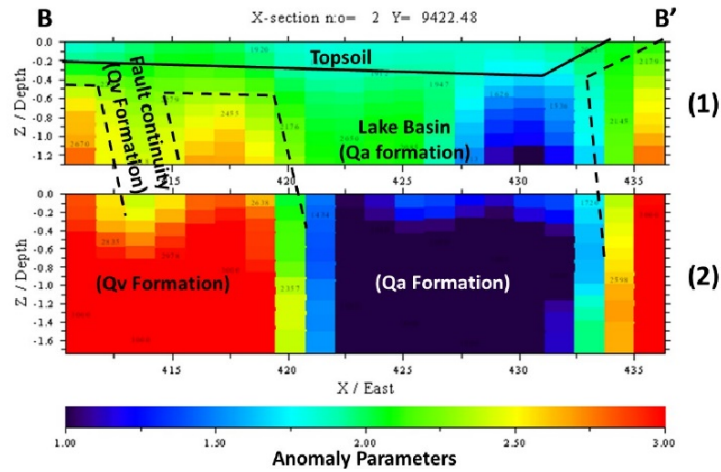


FIGURE 10. Cross-section of section B-B' data residual anomalies (1) and regional anomalies (2)

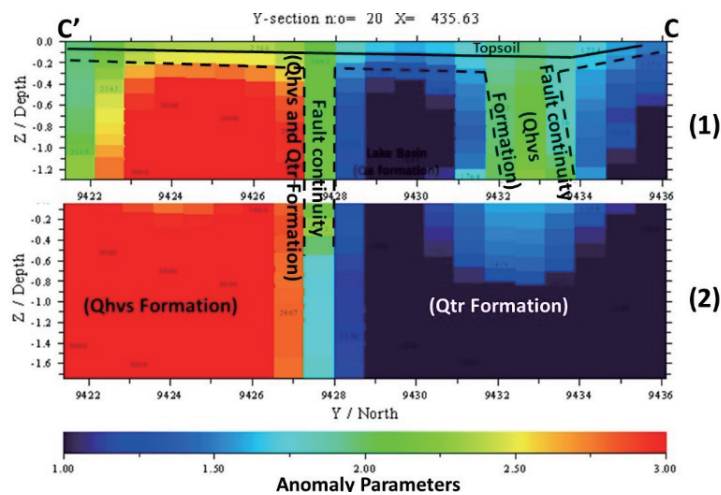


FIGURE 11. Cross-section of section C'-C data residual anomalies (1) and regional anomalies (2)

0.00-0.11 km depth, while the lower layer consists of high-density igneous rock (2.80-3.00 g/cm<sup>3</sup>) extending from area B to A (orange-red anomalies).

The second 2D cross-section, B-B', is located at Y = 9422.48 and passes through Batubrak Subdistrict (Qhvs formation) and Bandar Negeri Suoh Subdistrict (Qa, Qv formation). Figure 10 illustrates its residual and regional anomaly data. This section contains two northwest-southeast-oriented strike-slip faults, extending between longitudes 410-419 and 425-436, with depths ranging from 0.30 km in area A to 0.60 km in area B. These faults, associated with minor block subsidence and permeable rock formations (blue-green anomalies), contribute to the formation of Suoh Lake, a pull-apart basin depression spanning longitudes 419-426 at a depth of 0.40 km. The section's geological features align with the regional geology, acting as a structural control for nearby hot spring activity. The uppermost layer consists of topsoil, while the lower layer is characterized by igneous rock penetration.

The third 2D cross-section, C-C', is located at X = 435.63 and crosses the Sekincau sub-district (Qhvs formation), as shown in Figure 11 with residual and regional anomaly data. This section contains two northwest-southeast-oriented horizontal faults, spanning latitudes 9422-9427 and 9429-9436, with depths ranging from 0.30 km in area A to 0.20 km in area B. These faults, associated with minor block subsidence, transition from impermeable

(orange-red anomalies) to permeable rock formations (dark blue-light green anomalies). The fault at 9422-9427 contributes to the formation of a pull-apart basin depression and influences geothermal activity, as it intersects with the B-B' section. The fault at 9429-9436 serves as an entry point for geothermal fluids into the reservoir, estimated at depths of 1.20 km in area A and 1.60 km in area B, composed of low-density sandstone ( $1.48\text{--}1.76\text{ g/cm}^3$ ) with high porosity and permeability. The fluid is contained by a caprock layer at 0.20 km depth in area A, consisting of clay ( $1.72\text{--}2.38\text{ g/cm}^3$ ) with impermeable properties, preventing fluid escape except through surrounding fractures.

The fourth 2D cross-section, D-D', is located at  $Y = 9431.31$  and traverses the Batubrak (QTr), Bandar Negeri Suoh (Qv, QTr, Qhvs), and Sekincau (Qhvs) subdistricts, as shown in Figure 12 with residual and regional anomaly data. This section contains two faults: a northwest-southeast-oriented fault between longitudes 410-419 at a depth of 0.20 km in both areas A and B, and a northeast-southwest-oriented fault between longitudes 424-436 at depths of 0.30 km in area A and 0 km in area B. These faults cause minor block subsidence and occur in rock formations ranging from permeable (dark blue-light green anomalies) to impermeable (orange-red anomalies). The northwest-southeast fault is believed to influence geothermal energy potential and manifestations, while the northeast-southwest fault likely serves as a recharge zone, allowing meteoric water [24,25] to enter the reservoir due to its permeable rock formation. The uppermost layer consists of topsoil.

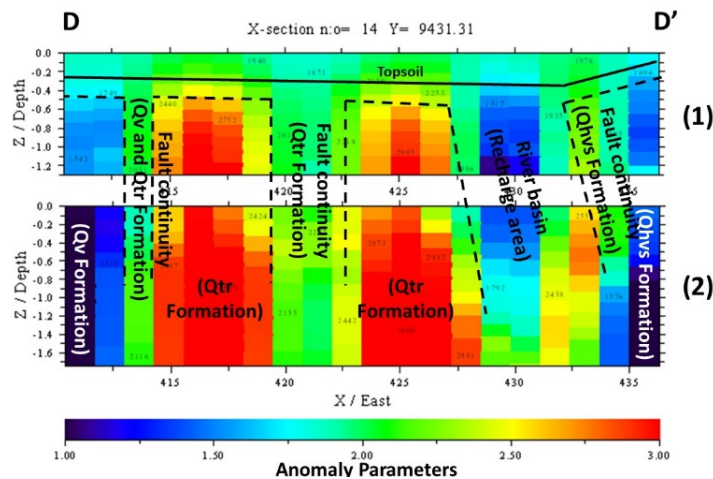


FIGURE 12. Cross-section of section D-D' data residual anomalies (1) and regional anomalies (2)

**4. Conclusion.** Research conducted in the East Sekincau region of Lampung Province, Indonesia, has successfully identified distinct gravity anomaly patterns within the geothermal system, categorized as low (light purple-dark blue), medium (light green-dark yellow), and high (orange-red). Through residual and regional anomaly modeling, significant rock density contrasts were revealed, with sedimentary rocks ranging from  $1.00$  to  $2.55\text{ g/cm}^3$ , medium-density igneous rocks from  $2.22$  to  $2.76\text{ g/cm}^3$ , and high-density igneous rocks from  $2.72$  to  $3.00\text{ g/cm}^3$ . The application of two-dimensional (2D) gravity data modeling proved effective in delineating subsurface structures, enabling the identification of fault zones, heat sources, and reservoir formations essential for geothermal energy extraction. Integrating geophysical modeling with multidisciplinary approaches enhances exploration accuracy and supports the efficient and sustainable utilization of natural energy resources. As an integral part of future development, further research is recommended to incorporate additional geophysical methods such as magnetic, seismic, and geoelectrical surveys to strengthen subsurface interpretations. Advancing toward three-dimensional (3D) gravity modeling will improve spatial resolution and precision in identifying geothermal prospects.

Moreover, the adoption of machine learning techniques for regional gravity data analysis, along with hydrogeological and geochemical studies, will provide deeper insights into fluid dynamics and reservoir characteristics. These strategies will optimize geothermal exploration in Indonesia and contribute to the global transition toward sustainable, data-driven energy solutions.

**Acknowledgment.** We thank the Physics Laboratory, Department of Physics, Institut Teknologi Sumatera, Indonesia for its facility and financial support.

## REFERENCES

- [1] H. W. Utama, R. Mulyasari and Y. M. Said, Geothermal potential on Sumatra fault system to sustainable geotourism in West Sumatra, *JGE (Jurnal Geofis. Eksplorasi)*, vol.7, no.2, pp.126-137, DOI: 10.23960/jge.v7i2.128, 2021.
- [2] S. Darma, Y. L. Imani, M. N. A. Shidqi, T. D. Riyanto and M. Y. Daud, Country update: The fast growth of geothermal energy development in Indonesia, *Proceeding World Geotherm. Congr. 2020+1*, no.12, pp.1-9, 2021.
- [3] M. Iqbal, M. A. Al-Hassan, N. R. Herdianita and B. R. Juliarka, Determining recharge area in ULUBELU geothermal field, LAMPUNG, Indonesia using stable isotope data, *Appl. Geochemistry*, vol.156, 105763, DOI: 10.1016/j.apgeochem.2023.105763, 2023.
- [4] M. Saparun, R. Akbar, M. Marbun, A. Dixit and A. Saxena, Application of induced polarization and resistivity to the determination of the location of minerals in extrusive rock area, southern mountains of Java, Indonesia, *Int. J. Hydrol. Environ. Sustain.*, vol.1, no.3, pp.108-119, DOI: 10.58524/ijhes.v1i3.137, 2022.
- [5] S. Liu, I. Suardi, X. Xu, S. Yang and P. Tong, The geometry of the subducted slab beneath Sumatra revealed by regional and teleseismic traveltime tomography, *J. Geophys. Res. Solid Earth*, vol.126, no.1, pp.1-29, DOI: 10.1029/2020JB020169, 2021.
- [6] M. Iqbal and B. A. Kusumasari, Deciphering the Way Ratai geothermal system, Lampung, Indonesia: A comprehensive geochemical and isotopic analysis, *Geothermics*, vol.119, DOI: 10.1016/j.geothermics.2024.102985, 2024.
- [7] M. Ali, A. Habib, S. Alawiyah and A. Santoso, *Identifikasi Persebaran Air Panas Bawah Permukaan Di Daerah Merak Batin, Natar, Lampung Selatan Menggunakan Data Magnetik Gradiometer Dan Geolistrik (Identification of Underground Hot Water Distribution in the Merak Batin Area, Natar, South Lampung Using Magnetic Gradiometer and Geophysical Data)*, Sumatra Institute of Technology, Indonesia, 2012.
- [8] S. Bronto, P. Asmoro, G. Hartono and S. Sulistiyono, Evolution of Rajabasa volcano in Kalianda area and its vicinity, South Lampung Regency, *Indones. J. Geosci.*, vol.7, no.1, pp.11-25, DOI: 10.17014/ijog.v7i1.132, 2012.
- [9] Triani, R. Umam and Sismanto, D modeling of subsurface Lawanopo fault in southeast Sulawesi, Indonesia using grablox and its consequence to geohazard, *Indones. J. Geogr.*, vol.53, no.1, pp.67-77, DOI: 10.22146/IJG.50878, 2021.
- [10] S. Maryanto, Geo techno park potential at Arjuno-Welirang volcano hosted geothermal area, Batu, East Java, Indonesia (Multi geophysical approach), *AIP Conf. Proc.*, vol.1908, DOI: 10.1063/1.5012712, 2017.
- [11] C. F. Li, An integrated geodynamic model of the Nankai subduction zone and neighboring regions from geophysical inversion and modeling, *J. Geodyn.*, vol.51, no.1, pp.64-80, DOI: 10.1016/j.jog.2010.08.003, 2011.
- [12] A. Watlet et al., Gravity monitoring of underground flash flood events to study their impact on groundwater recharge and the distribution of karst voids, *Water Resour. Res.*, vol.56, no.4, pp.1-18, DOI: 10.1029/2019WR026673, 2020.
- [13] R. Umam, K. Cengiz and A. Said, Application of major and trace elements for detecting the origin of groundwater: Lithium enrichment in Ain Al-Harrah hot spring influenced by Red Sea, Saudi Arabia, *Int. J. Hydrol. Environ. Sustain.*, vol.3, no.3, pp.151-162, 2024.
- [14] R. Umam, M. Tanimizu, H. Nakamura, Y. Nishio, R. Nakai, N. Sugimoto, Y. Mori, Y. Kobayashi, A. Ito, S. Wakaki, K. Nagaishi and T. Ishikawa, Lithium isotope systematics of Arima hot spring waters and groundwaters in Kii Peninsula, *Geochem. J.*, vol.56, no.5, pp.E8-E17, DOI: 10.2343/geochemj.GJ22015, 2022.
- [15] R. Umam, R. Junaidi, M. Syazali, F. Farid, A. Saregar and A. Andiyan, Optimization of piper trilinear diagram using lithium isotope systematics: An application for detecting the contribution of

- geothermal water from Aso caldera after earthquake 2016 in Kumamoto aquifer, Japan, *Indones. J. Sci. Technol.*, vol.10, no.1, pp.159-170, 2025.
- [16] K. C. S. Dewi, R. N. Siregar, T. I. Ningati, Z. N. Pulungan, A. Indriyawati and H. Takahashi, Analysis of subsurface faults using 3D gravity method based on satellite image data: Insights into Indo-Australian and Eurasian Plate subduction in the formation of an accretionary prism, *Int. J. Hydrol. Environ. Sustain.*, vol.4, no.3, pp.135-148, DOI: 10.58524/ijhes.v4i3.960, 2025.
- [17] M. F. Ismullah, M. A. Massinai and Maria, Shallow depth study using gravity & magnetics data in central Java-Yogyakarta, *IOP Conf. Ser. J. Phys. Conf. Ser.*, vol.979, 012046, DOI: 10.1088/1742-6596/979/1/012046, 2018.
- [18] D. C. Fraser, Countouring of VLF-EM data, *Geophysics*, vol.34, pp.958-967, 1969.
- [19] L. Rybach, J. Wilhelm and H. Gorhan, Geothermal use of tunnel waters – A Swiss speciality, *Int. Geotherm. Conf.*, pp.17-23, [https://www.researchgate.net/publication/237285547\\_Geothermal\\_use\\_of\\_tunnel\\_waters\\_-\\_a\\_Swiss\\_speciality](https://www.researchgate.net/publication/237285547_Geothermal_use_of_tunnel_waters_-_a_Swiss_speciality), 2003.
- [20] Y. Wang, J. Xu, J. Xu and C. Zhong, Estimation of rock burst grades using rock mass strength, *Adv. Civ. Eng.*, DOI: 10.1155/2020/2517459, 2020.
- [21] R. Umam, Sismanto and H. Takahashi, Interpretation of 2 dimensional very low frequency electromagnetic (VLF-EM) data of an underground river using a 2LAYINV Markku's software, *ICIC Express Letters, Part B: Applications*, vol.16, no.5, pp.527-538, DOI: 10.24507/icicelb.16.05.527, 2025.
- [22] R. Xu and L. Wang, The horizontal-to-vertical spectral ratio and its applications, *EURASIP J. Adv. Signal Process.*, no.1, DOI: 10.1186/s13634-021-00765-z, 2021.
- [23] R. A. T. Listyani, I. A. Prabowo and A. A. De Jesus, Aquifer potential analysis based on hydrostratigraphy and geological lineament in Kokap Region, Kulon Progo, Yogyakarta, Indonesia, *Int. J. Hydrol. Environ. Sustain.*, vol.2, no.2, pp.50-64, DOI: 10.58524/ijhes.v2i2.197, 2023.
- [24] Z. Sabara, I. N. Afiah and R. Umam, Integration of green ergonomics in robust decision making approach in water resources management in Makassar city, *Int. J. Technol.*, vol.13, no.2, pp.264-273, DOI: 10.14716/ijtech.v13i2.5113, 2022.
- [25] M. Nissar, K. N. Chethan, Y. A. Birjerane, S. Patil, S. Shetty and A. Das, Coconut coir fiber composites for sustainable architecture: A comprehensive review of properties, processing, and applications, *Journal of Composites Science*, pp.1-24, 2025.